

# Ray-based description of mode coupling by sound speed fluctuations in the ocean

A.L. Virovlyansky

Institute of Applied Physics, Russian Academy of Science,

46, Ulyanova St., Nizhny Novgorod, Russia, 603950

viro@hydro.appl.sci-nnov.ru

July 16, 2014

## Abstract

A traditional approach to the analysis of mode coupling in a fluctuating underwater waveguide is based on solving the system of coupled equations for the second statistical moments of mode amplitudes derived in the Markov approximation [D.B. Creamer, J. Acoust. Soc. Am. 99, 2825–2838 (1996)]. In the present work an alternative approach is considered. It is based on an analytic solution of the mode coupling equation derived in the high frequency approximation [A.L. Virovlyanskii and A.G. Kosterin, Sov. Phys. Acoust. 35, 138–142 (1987)]. This solution representing the mode amplitude as a sum of contributions from two geometrical rays is convenient for statistical averaging. It allows one to easily derive analytical expressions for any statistical moments of mode amplitudes. The applicability of this approach is demonstrated by comparing its predictions for a deep water acoustic waveguide with results of full wave numerical simulation carried out using the method of wide angle parabolic equation.

**PACS numbers:** 43.30.Bp, 43.30.Dr, 43.30.Re, 43.60.Cg

# I Introduction

An environmental model representing an unperturbed range-independent waveguide with weak sound speed fluctuations is widely used in solving different problems of ocean acoustics [1, 2]. The sound field in this model can be decomposed into a sum of normal modes of the unperturbed waveguide with complex amplitudes  $a_m$  being random functions of range  $r$ . Mode coupling by the sound speed fluctuations is quantitatively described by statistical moments of mode amplitudes  $\langle a_m a_n^* \rangle$  where the asterisk denotes complex conjugation and the angular brackets denote statistical averaging. A traditional approach to the analysis of the modal structure of the sound field in a fluctuating waveguide is based on solving the transport equations for moments  $\langle a_m a_n^* \rangle$  [3–8].

Complete system of transport equations derived in the Markov approximation includes  $M^2$  linear differential equations, where  $M$  is the number of propagating modes [6, 8]. A truncated version of this system including only  $M$  equations for the mean mode intensities  $\langle |a_m|^2 \rangle$  – they are called the master equations – was derived in Ref. [4] under assumption that the cross-mode coherences, that is, the moments  $\langle a_m a_n^* \rangle$  with  $m \neq n$ , are negligible.

In Ref. [8] all the statistical moments  $\langle a_m a_n^* \rangle$  were calculated numerically for a deep water acoustic waveguide with sound speed fluctuations induced by random internal waves. It turned out that the values of  $|\langle a_m a_n^* \rangle|$  for close, but not equal,  $m$  and  $n$  are of the same order of magnitude as  $\langle |a_m|^2 \rangle^{1/2} \langle |a_n|^2 \rangle^{1/2}$  and the mean intensities and cross-mode coherences ‘evolve over similar range scales’. This contradicts the assumption about the smallness of the cross-mode coherences made when deriving the master equations. In spite of this fact, the numerical simulation demonstrated that the solutions of master equations provide good estimates of mean mode intensities  $\langle |a_m(r)|^2 \rangle$ . However, it should be noticed that these solutions are smooth functions of range and they do not predict small oscillations of  $\langle |a_m(r)|^2 \rangle$  with range found by solving the complete system of all the  $M^2$  equations. Similar results were obtained in Refs. [9, 10] for a shallow water waveguide.

In the present paper we consider an alternative approach to examining the mode coupling. It was derived in Ref. [11] (see also Refs. [12–15]) in the study of ray-mode relations in a waveguide with weak sound-speed fluctuations. This approach is based on a surprisingly simple analytical solution of the mode coupling equation obtained in the high frequency approximation. It expresses the mode amplitude through parameters of two geometrical rays which we call the mode rays. This estimate of  $a_m$  is an analog of the well-known formula

of geometrical optics describing the variation of complex ray amplitude in the presence of weak inhomogeneities of refractive index. The ray-based estimate of mode amplitude is convenient for statistical averaging. Analytical expressions for any statistical moments of mode amplitudes, including joint moments of amplitudes at different frequencies, are readily follow from this formula.

We also consider a simplified expression for the mean mode intensity obtained by averaging the parameters of the ray-based estimate of  $\langle |a_m|^2 \rangle$  over the ray cycle length. It is shown that in the high frequency limit this expression, describing a smoothed range-dependence of the mean mode intensity, satisfies the master equations. This fact agrees with numerical result of Refs. [8–10].

A weak point of our analytical approach is insufficient knowledge about the limits of its applicability. So far, its predictions have never been compared to results of full wave simulation. In the present paper such a comparison is made for an environmental model similar to that used in Ref. [8]. Sound field excited by a points source at a frequency of 100 Hz was calculated numerically using the method of wide angle parabolic equation in 360 realizations of the fluctuating waveguide. Mode amplitudes were found by projecting computed wave fields onto eigenfuntions of the unperturbed waveguide. Parabolic equation based (pe-based) estimates obtained in this way are compared with the ray-based estimates found by evaluating mode amplitudes in the same realizations of the waveguide using our approximate analytical solution of the mode coupling equation. Estimates of statistical moments were computed by the Monte Carlo method, that is, by averaging the products of mode amplitudes over all the realizations of random waveguide. The comparison has demonstrated a good agreement between the pe-based and ray-based results.

Numerical simulation have shown that the ray-based approach properly describes not only the smoothed range-dependencies of statistical moments of mode amplitudes but the small oscillations of these moments ("missed" by the master equations), as well. These oscillations were predicted in Ref. [12] where it was shown that the jump-like variations of the mode amplitude and its statistical moments occur in the neighborhood of the upper turning points of the mode rays.

As in Refs. [4, 6, 8–10], we neglect the horizontal refraction of sound waves and consider a two-dimensional environmental model. Out-of-plane wave scattering was taken into account in Refs. [16, 17].

The organization of this paper is as follows.

Analytical relation expressing the mode amplitude through parameters of two ray paths is presented in Sec. II. Section III gives analytical expressions for a few statistical moments of mode amplitudes derived using this relation. In Sec. IV, it is shown that in the limit of high frequency the ray-based estimate of the mean mode intensity  $\langle |a_m|^2 \rangle$  whose parameters are smoothed over the ray cycle length satisfies the master equations. Section V presents results of numerical simulation in a deep water waveguide with sound speed fluctuations induced by random internal waves. It is demonstrated that the predictions of our ray-based approach agree with the results of simulation carried out using the method of wide angle parabolic equation. In Sec. VI, the results of this work are summarized.

## II Analytical description of mode amplitudes in the presence of weak sound speed fluctuations

In this section we present a simple analytical approach derived in Refs. [11, 14, 15] for a ray-based description of mode amplitudes in a waveguide with weak large scale sound speed fluctuations. It is assumed that the wave field is excited by a point source.

### A Mode representation of the wave field

Consider a two dimensional model of underwater sound channel with the sound speed field  $c(r, z) = \bar{c}(z) + \delta c(r, z)$ , where  $r$  is the distance,  $z$  is the depth,  $\bar{c}(z)$  is the unperturbed sound speed profile, and  $\delta c(r, z)$  is the weak range-dependent perturbation. The refractive index is  $\nu(r, z) = c_0/c(r, z)$ , where  $c_0$  is the reference sound speed. We assume that  $|c(r, z) - c_0| \ll c_0$ . Due to the weakness of perturbation

$$\nu(r, z) = \bar{\nu}(z) + \delta\nu(r, z),$$

where

$$\bar{\nu}(z) = \frac{c_0}{\bar{c}(z)}, \quad \delta\nu(r, z) = -\frac{c_0}{\bar{c}^2(z)}\delta c(r, z).$$

We assume that the perturbation  $\delta c(r, z)$  is a zero mean Gaussian random field with the correlation function

$$\langle \delta c(r_1, z_1) \delta c(r_2, z_2) \rangle = K(\xi, \zeta, Z), \quad (1)$$

where

$$\xi = r_1 - r_2, \quad \zeta = z_1 - z_2, \quad Z = (z_1 + z_2)/2.$$

Note that

$$K(\xi, \zeta, Z) = K(-\xi, \zeta, Z). \quad (2)$$

Characteristic scales of correlation function  $K$  along the coordinates  $\xi$  and  $\zeta$  denote  $\Delta_\xi$  and  $\Delta_\zeta$ , respectively.

The acoustic pressure field  $u(r, z)$  at a carrier frequency  $f$  can be expressed as

$$u(r, z) = \sum_{m=1}^M \sqrt{\frac{2\pi i}{k_m r}} a_m(r) \varphi_m(z) e^{ik_m r}, \quad (3)$$

where  $k_m$  and  $\varphi_m(z)$  are eigenvalues and eigenfunctions of the Sturm-Liouville problem in the unperturbed (range-independent) waveguide, respectively [2, 18]. For simplicity, it is assumed that the sum (3) includes only those modes whose turning points are located within the water bulk. This assumption will simplify the use of the WKB approximation for description of  $k_m$  and  $\varphi_m(z)$ .

In what follows we will consider the wave field excited by a point source set at  $r = 0$  and  $z = z_0$ . In this case,  $a_m(0) = \varphi_m(z_0)$ .

In the WKB approximation the eigenvalues can be presented as  $k_m = kh_m$ , where  $k = 2\pi f/c_0$  is a reference wavenumber and  $h_m$  is determined by the quantization rule [2]

$$k \int_{z_{\min}}^{z_{\max}} dz \sqrt{\bar{\nu}^2(z) - h_m^2} = \pi(m - 1/2) \quad (4)$$

with  $z_{\min}$  and  $z_{\max}$  being the mode turning depths. In this approximation the  $m$ -th mode is associated with a ray path whose grazing angle at depth  $z$ ,  $\theta_m(z)$ , is determined by the relation  $h_m = \bar{\nu}(z) \cos \theta_m(z)$ .

The cycle length (period) of this ray path is given by

$$D_m = 2h_m \int_{z_{\min}}^{z_{\max}} \frac{dz}{\sqrt{\bar{\nu}^2(z) - h_m^2}} = 2 \int_{z_{\min}}^{z_{\max}} \frac{dz}{\tan(\theta_m(z))}. \quad (5)$$

A 'differential' form of the quantization rule follows from Eqs. (4) and (5) as

$$\frac{dh_m}{dm} = -\frac{2\pi}{kD_m}. \quad (6)$$

The eigenfunction  $\varphi_m(z)$  in the WKB approximation [2] can be presented in the form

$$\varphi_m(z) = \varphi_m^+(z) + \varphi_m^-(z), \quad (7)$$

where

$$\varphi_m^\pm(z) = q_m(z) e^{\pm i[kg_m(z) - \pi/4]}, \quad (8)$$

$$q_m(z) = \frac{h_m^{1/2}}{[\bar{\nu}^2(z) - h_m^2]^{1/4} D_m^{1/2}} = \frac{1}{[D_m \tan \theta_m(z)]^{1/2}}, \quad (9)$$

$$g_m(z) = \int_{z_{\min}}^z dz \sqrt{\bar{\nu}^2(z) - h_m^2}. \quad (10)$$

Functions  $\varphi_m^\pm(z)$  represent two quasi-plane waves called the Brillouin waves.

Note a useful relation following from Eqs. (4) and (10)

$$k \frac{\partial g_m(z)}{\partial m} = \frac{2\pi}{D_m} \int_{z_{\min}}^z \frac{dz}{\tan(\theta_m(z))}. \quad (11)$$

## B Geometrical optics for modes

Within the framework of standard geometrical optics, the influence of a weak sound speed perturbation  $\delta c$  with spatial scales significantly exceeding the wavelength can be accounted for using a well-known approximate formula. If in the unperturbed medium the contribution of a sound ray to the total field  $u$  is  $A \exp(ikS)$ , where  $A$  and  $S$  are the ray amplitude and eikonal, respectively, then in the presence of perturbation its contribution becomes [1, 2]

$$u = A e^{ik(S+X)}, \quad (12)$$

where

$$X = \int_{\Gamma} \delta \nu \, ds, \quad (13)$$

$ds$  is the arc length and the integration goes over the unperturbed ray path  $\Gamma$ . Although this formula is valid only at relatively short ranges it is widely used in the ocean acoustics [1]. In particular, it is used in solving the inverse problem in the classical scheme of ocean acoustic tomography [19].

In Ref. [11] (see also Refs. [12–15]) it is shown that there exists a close analog of Eq. (12) for normal modes. The point is that the  $m$ -th mode constructively interferes (adds in phase) with neighboring modes along the trajectories of two unperturbed rays leaving the source

at launch angles  $\pm\theta_m(z_0)$  which are equal to grazing angles of the Brillouin waves  $\varphi_m^\pm(z)$  at the source depth. As in Refs. [11–15], we shall call these rays the mode rays and denote their trajectories  $z_m^\pm(r)$ . Note that for a given  $m$  the angle  $\theta_m(z_0)$  is a function of the carrier frequency  $f$ . This makes the trajectories  $z_m^\pm(r)$  frequency dependent. Denote the grazing angles of the ray paths  $z_m^\pm(r)$  at range  $r$  by  $\chi_m^\pm(r)$ , so that  $dz_m^\pm(r)/dr = \tan \chi_m^\pm(r)$ . Both mode rays have the same cycle length given by Eq. (5). Examples of mode rays are shown in Fig. 1. It graphs trajectories  $z_m^\pm(r)$  for the 36-th mode in the canonical sound speed profile at a carrier frequency of 100 Hz.

In the presence of perturbation  $\delta c(r, z)$  the mode amplitude is expressed by the approximate formula

$$a_m(r) = \varphi_m^+(z_0)e^{ikX_m^+(r)} + \varphi_m^-(z_0)e^{ikX_m^-(r)}, \quad (14)$$

with

$$X_m^\pm = \int_{\Gamma_m^\pm} ds \, \delta\nu, \quad (15)$$

where the integration goes along the trajectories of mode rays  $\Gamma_m^\pm$  [11, 15]. Equation (15) can be written in the form

$$X_m^\pm(r) = \int_0^r \frac{dr'}{\cos \chi_m^\pm} \delta\nu(r, z_m^\pm(r)). \quad (16)$$

Formula (14) is derived under the same assumptions as its prototype for the ray amplitude (12). The simplest derivation of Eq. (14) consists in projecting the ray representation of the wave field onto eigenfunctions of the unperturbed waveguide with the evaluation of arising integrals using the stationary phase technique [14, 15]. Therefore Eq. (14) should have approximately the same range of applicability as Eq. (12).

A more accurate and general expression for the mode amplitude can be derived proceeding from the ray representation of the wave field in a range-dependent waveguide [20–22]. Besides, Eq. (14) can be generalized in a different direction. In Ref. [11, 14, 15], a more general version of this formula was derived which can be used for description of wave diffraction by sound speed fluctuations. In these works, the notion of Fresnel zones for modes is introduced which is analogous to the usual Fresnel zones introduced for rays.

In the present paper the indicated generalizations are not considered. All our subsequent analysis is based on formula (14).

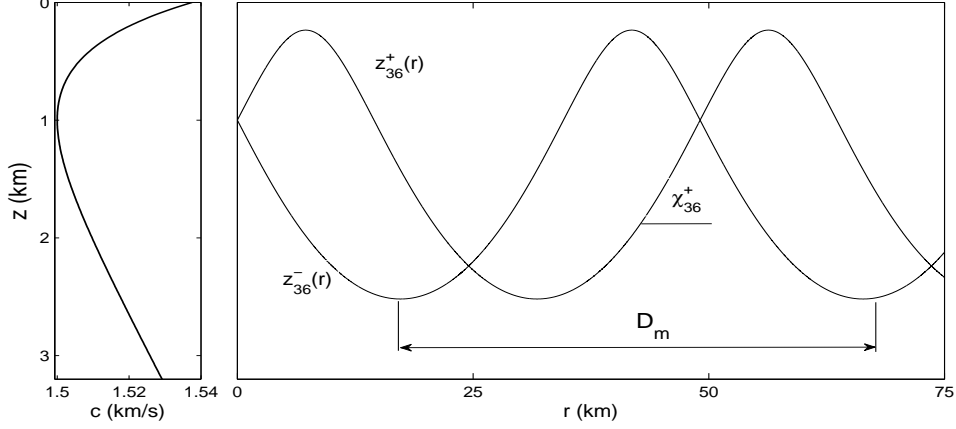


Figure 1: Left panel: canonical sound speed profile. Right panel: trajectories of the mode rays of the 36-th mode at a carrier frequency of 100 Hz.

### III Statistical moments of mode amplitudes

Since  $X_m^\pm(r)$  are zero mean Gaussian random functions, an analytical expression for any statistical moment of mode amplitudes is readily derived from Eq. (14) using the well-known formula  $\langle e^{i\alpha} \rangle = -e^{-\langle \alpha^2 \rangle / 2}$  for a zero mean Gaussian random variable  $\alpha$ . The mean value (coherent component) of the mode amplitude  $a_m$  is

$$\langle a_m \rangle = \Phi_m^+ e^{-\frac{k^2}{2} \langle (X_m^+)^2 \rangle} + \Phi_m^- e^{-\frac{k^2}{2} \langle (X_m^-)^2 \rangle}, \quad (17)$$

where  $\Phi_m^\pm = \varphi_m^\pm(z_0)$ .

The cross-mode coherence is given by

$$\begin{aligned} \langle a_m a_n^* \rangle &= \Phi_m^+ \Phi_n^- e^{-\frac{k^2}{2} \langle (X_m^+ - X_n^+)^2 \rangle} + \Phi_m^+ \Phi_n^+ e^{-\frac{k^2}{2} \langle (X_m^+ - X_n^-)^2 \rangle} \\ &+ \Phi_m^- \Phi_n^- e^{-\frac{k^2}{2} \langle (X_m^- - X_n^+)^2 \rangle} + \Phi_m^- \Phi_n^+ e^{-\frac{k^2}{2} \langle (X_m^- - X_n^-)^2 \rangle}. \end{aligned} \quad (18)$$

In the particular case  $m = n$ , Eq. (18) gives an expression for the mean mode intensity

$$\langle |a_m|^2 \rangle = 2Q_m^2 \left[ 1 + e^{-\frac{k^2}{2} \langle (X_m^+ - X_m^-)^2 \rangle} \sin(2kG_m) \right], \quad (19)$$

where

$$Q_m = q_m(z_0) = \frac{1}{[D_m \tan \theta_m(z_0)]^{1/2}},$$



$$G_m = g_m(z_0) = \frac{2\pi}{D_m} \int_{z_{\min}}^{z_0} \frac{dz}{\tan(\theta_m(z))}.$$

An expression for the mean squared intensity (the fourth moment of mode amplitude) is

$$\begin{aligned} \langle |a_m|^4 \rangle = Q_m^4 & \left[ 6 + 8 \sin(2kG_m) e^{-\frac{k^2}{2} \langle (X_m^+ - X_m^-)^2 \rangle} \right. \\ & \left. - 2 \cos(4kG_m) e^{-2k^2 \langle (X_m^+ - X_m^-)^2 \rangle} \right]. \end{aligned} \quad (20)$$

It is clear that similar formulas are readily derived for the joint statistical moments of mode amplitudes at different frequencies.

In the scope of our ray-based approach, all the moments of mode amplitudes are expressed through  $\langle X_m^\pm X_n^\mp \rangle$  and  $\langle X_m^\pm X_n^\pm \rangle$ . Evaluation of these quantities is simplified under the assumption that the horizontal correlation scale of sound speed fluctuations,  $\Delta_r$ , is substantially less than the cycle length  $D_m$ . Then, at ranges  $r \gg \Delta_r$  the mode rays cross uncorrelated inhomogeneities, the quantities  $X_m^+$  and  $X_m^-$  become statistically independent, and  $\langle X_m^\pm X_n^\mp \rangle = 0$ .

Explicit expression for the dispersions of  $X_m^\pm$  is given by

$$\begin{aligned} \langle (X_m^\pm)^2 \rangle = \int_0^r \int_0^r & \frac{dr' dr''}{g_m(r') g_m(r'')} \\ & \times K \left( r' - r'', z_m^\pm(r') - z_m^\pm(r''), \frac{1}{2} (z_m^\pm(r') + z_m^\pm(r'')) \right), \end{aligned} \quad (21)$$

where  $g_m(r) = \bar{c}(z_m^\pm(r)) \cos(\chi_m^\pm(r))$ . Let us change the variables of integration from  $(r', r'')$  to  $(r', \xi)$ , where  $\xi = r' - r''$ . The main contribution to the integral comes from the interval  $|\xi| < \Delta_\zeta$ . Since  $\Delta_\zeta$  is small compared to  $D_m$ , we can use the approximations  $z_m^\pm(r') - z_m^\pm(r'') \simeq \xi \tan \chi_m^\pm(r')$  and  $(z_m^\pm(r') + z_m^\pm(r''))/2 \simeq z_m^\pm(r')$ . At ranges  $r \gg \Delta_\zeta$  we can formally extend the limits of integration over  $\xi$  to infinity. Then Eq. (21) translates to

$$\langle (X_m^\pm)^2 \rangle = \int_0^r \frac{dr'}{\bar{c}^4(z_m^\pm(r')) \cos^2 \chi_m^\pm(r')} \int_{-\infty}^{\infty} d\xi K(\xi, \xi \tan \chi_m^\pm(r'), z_m^\pm(r')). \quad (22)$$

Since the trajectories  $z_m^+(r)$  and  $z_m^-(r)$  differ only by a shift along the  $r$ -axis, the contribution to the integral over  $r'$  from any interval of length  $D_m$  is the same for both mode rays. It is easy to see that for an arbitrary function  $F(z_m^\pm(r'), |\chi_m^\pm(r')|)$  we have the relation

$$\frac{1}{D_m} \int_{r_1}^{r_1 + D_m} dr' F(z_m^\pm(r'), |\chi_m^\pm(r')|) = \frac{2}{D_m} \int_{z_{\min}}^{z_{\max}} \frac{dz}{\tan \theta_m(z)} F(z, \theta_m(z)).$$

At ranges  $r = ND_m$  with  $N$  being an integer

$$\langle (X_m^+)^2 \rangle = \langle (X_m^-)^2 \rangle = \langle X_m^2 \rangle, \quad (23)$$

where

$$\langle X_m^2 \rangle = r \frac{2}{D_m} \frac{c_0^2 k^2}{k_m^2} \int_{z_{\min}}^{z_{\max}} \frac{dz}{\bar{c}^6(z) \tan \theta_m(z)} \int_{-\infty}^{\infty} d\xi K(\xi, \xi \tan \theta_m(z), z). \quad (24)$$

In deriving this formula we have taken into account that due to Snell's law  $\cos \chi_m^\pm = (k_m/k)(\bar{c}(z_m^\pm)/c_0)$ . At an arbitrary range  $r$ , not necessary multiple of  $D_m$ , Eq. (24) gives a smoothed estimate of  $\langle (X_m^+)^2 \rangle$  and  $\langle (X_m^-)^2 \rangle$ .

Let us slightly simplify formulas (17) – (19) neglecting the differences between  $\langle (X_m^+)^2 \rangle$  and  $\langle (X_m^-)^2 \rangle$  and between  $\langle (X_m^+ - X_n^+)^2 \rangle$  and  $\langle (X_m^- - X_n^-)^2 \rangle$ . Assuming that  $\langle X_m^\pm X_m^\mp \rangle = 0$  and replacing  $\langle (X_m^\pm)^2 \rangle$  by  $\langle (X_m)^2 \rangle$  and  $\langle (X_m^\pm - X_n^\pm)^2 \rangle$  by  $\langle (X_m - X_n)^2 \rangle$ , we find

$$\langle a_m \rangle = \varphi_m(z_0) e^{-\frac{k^2}{2} \langle X_m^2 \rangle}, \quad (25)$$

$$\begin{aligned} \langle a_m a_n^* \rangle &= 2Q_m Q_n \left[ e^{-\frac{k^2}{2} \langle (X_m - X_n)^2 \rangle} \cos(k(G_m - G_n)) \right. \\ &\quad \left. + e^{-\frac{k^2}{2} (\langle X_m^2 \rangle + \langle X_n^2 \rangle)} \sin(k(G_m + G_n)) \right], \end{aligned} \quad (26)$$

$$\langle |a_m|^2 \rangle = 2Q_m^2 \left[ 1 + e^{-k^2 \langle X_m^2 \rangle} \sin(2kG_m) \right], \quad (27)$$

and

$$\begin{aligned} \langle |a_m|^4 \rangle &= Q_m^4 \left[ 6 + 8 \sin(2kG_m) e^{-k^2 \langle X_m^2 \rangle} \right. \\ &\quad \left. - 2 \cos(4kG_m) e^{-4k^2 \langle X_m^2 \rangle} \right]. \end{aligned} \quad (28)$$

The value of  $\langle X_m^2 \rangle$  is given by Eq. (24). We do not present an explicit expression for  $\langle (X_m - X_n)^2 \rangle$ . When using Eq. (26),  $\exp \left[ -\frac{k^2}{2} \langle (X_m - X_n)^2 \rangle \right]$  should be replaced by any of two close functions  $\exp \left[ -\frac{k^2}{2} \langle (X_m^\pm - X_n^\pm)^2 \rangle \right]$ .

## IV Ray-based approach and master equations

The equations for statistical moments  $\langle a_m a_n^* \rangle$  are derived in the Markov approximation proceeding from the mode coupling equation [4, 6, 8]

$$\frac{da_m}{dr} = i \sum_{n=1}^M \rho_{mn} a_n e^{ik_{nm}r}, \quad (29)$$

where  $k_{nm} = k_n - k_m$ ,

$$\rho_{mn}(r) = \frac{k^2}{\sqrt{k_m k_n}} \int dz \varphi_m(z) \mu(r, z) \varphi_n(z), \quad (30)$$

$$\mu(r, z) = -\frac{c_0^2}{\bar{c}^3(z)} \delta c(r, z). \quad (31)$$

Note that our main formula (14) is an approximate solution of Eq. (29) [11].

In Refs. [8–10], it was shown that the numerical solution of the complete system of equations for all the moments  $\langle a_m a_n^* \rangle$  give practically the same result as the evaluation of these moments in the Monte Carlo simulation based on numerical solving the mode coupling equation (29) for different realizations of random perturbation  $\delta c(r, z)$ . This was the expected result. An unexpected result was that even though the cross-mode coherences were not small, the master equations properly predicted the smoothed mode intensities. In this section we will show that this result follows from our ray-based estimates of statistical moments. Namely, it will be shown that Eq. (27) obtained by smoothing the range-dependent parameters of Eq. (19), in the limit of high frequency gives a solution to the master equations.

In the notation of Refs. [8–10] the master equations have the form

$$\frac{d \langle |a_m|^2 \rangle}{dr} = 2 \sum_{n=0}^M \text{Re} (I_{mn, nm}) (\langle |a_n|^2 \rangle - \langle |a_m|^2 \rangle), \quad (32)$$

where  $I_{mn, nm}$  are the elements of the scattering matrix defined by the relations

$$I_{mn, qp} = \int_0^\infty d\xi \Delta_{mn, qp}(\xi) e^{ik_{pq}\xi} \quad (33)$$

and

$$\Delta_{mn, pq}(r - r') = \langle \rho_{mn}(r) \rho_{pq}(r') \rangle. \quad (34)$$

According to Eqs. (30), (31), and (34),

$$\Delta_{mn, nm}(\xi) = \frac{k^4 c_0^4}{k_n k_m} \int dz dz' \varphi_n(z) \varphi_n(z')$$

$$\times \frac{K(\xi, z - z', (z + z')/2)}{\bar{c}^3(z) \bar{c}^3(z')} \varphi_m(z) \varphi_m(z'). \quad (35)$$

At high frequencies, where the wavelength is small compared to the spatial scales of perturbation  $\delta c$ , we deal with the small-angle forward scattering of sound waves, and each mode couples mainly into modes with close numbers. This means that the main contribution to the sum in the right hand side of Eq. (29) comes from terms with  $n$  close to  $m$ . Using Eq. (7), we present the product of two eigenfunctions with close  $m$  and  $n$  in the form

$$\varphi_n(z) \varphi_m(z) \simeq q_m^2(z) \{e^{ik[g_n(z) - g_m(z)]} + c.c.\}, \quad (36)$$

where  $c.c.$  denotes the complex conjugate of the preceding term. In the right hand side of Eq. (36) we have omitted rapidly oscillating terms whose contributions to the integral in Eq. (35) are negligible. The integrand on the right of Eq. (35) is non-negligible only for  $|z - z'| = O(\Delta_\zeta)$ . We assume that the vertical scale of perturbation  $\Delta_\zeta$  is small compared to the depth interval between turning points of the  $m$ -th mode. Then the Brillouin waves within the depth interval of width  $\Delta_\zeta$  can be approximated by plane waves. Substitute Eq. (36) in Eq. (35) and drop the rapidly oscillating terms. Using Eqs. (6) and (11), the phases of the remaining terms can be represented as

$$\begin{aligned} k[g_n(z) - g_m(z) - g_n(z') + g_m(z')] &\simeq k \frac{\partial^2 g_m(z)}{\partial z \partial m} (n - m)(z' - z) \\ &= \frac{2\pi(n - m)(z - z')}{D_m} \cot \theta_m(z). \end{aligned}$$

In the resulting expression, we approximately replace  $n$  and  $z'$  in the pre-exponential factors by  $m$  and  $z$ , respectively. This yields

$$\begin{aligned} \Delta_{nm,mn}(\xi) &= \frac{k^4 c_0^4}{k_m^2} \int_{z_{\min}}^{z_{\max}} dz \int_{-\infty}^{\infty} d\zeta \\ &\times \frac{K(\xi, \zeta, z)}{\bar{c}^6(z) D_m^2 \tan^2 \theta_m(z)} \left[ e^{\frac{2\pi i(n-m)}{D_m} \zeta \cot \theta_m(z)} + c.c. \right]. \end{aligned} \quad (37)$$

Let us plug Eq. (37) into Eq. (33) and use the relation  $k_{nm} = 2\pi(m - n)/D_m$  which follows from Eq. (6). At high frequencies, the number of propagating mode becomes very large and the sum  $\sum_n \dots$  in Eq. (32) can be approximately replaced by the integral  $\int dn \dots$ . For  $m$  satisfying the condition  $1 \ll m \ll M$ , we will use the approximate relation

$$\int_0^M dn \exp \left[ \frac{2\pi i(m - n)}{D_m} (\xi \pm \zeta \cot \theta_m) \right] = D_m \delta(\xi \pm \zeta \cot \theta_m).$$

Then

$$\begin{aligned} \sum_{n=0}^M \operatorname{Re} I_{mn,nm} &= \int_0^\infty d\xi \int_0^M dn \Delta_{mn,nm}(\xi) \cos \left[ \frac{2\pi i (n-m)}{D_m} \xi \right] \\ &= \frac{k^4 c_0^4}{k_m^2 D_m} \int \frac{dz}{\bar{c}^6(z) \tan \theta_m(z)} \int_0^\infty d\xi [K(\xi, \xi \tan \theta_m, z) + K(\xi, -\xi \tan \theta_m, z)]. \end{aligned} \quad (38)$$

From the comparison of this expression with Eq. (24) (taking into account Eq. (2)) we find

$$2 \sum_{n=0}^M \operatorname{Re} (I_{mn,nm}) = k^2 \frac{d \langle X_m^2 \rangle}{dr}. \quad (39)$$

Plugging Eq. (27) into the left-hand side (l.h.s.) and right-hand side (r.h.s.) of Eq. (32) yields:

$$\text{l.h.s.} = 2k^2 Q_m^2 \sin(2kG_m) e^{-k^2 \langle X_m^2 \rangle} \frac{d \langle X_m^2 \rangle}{dr}, \quad (40)$$

and

$$\text{r.h.s.} = A + B + C, \quad (41)$$

where

$$A = 4Q_m^2 e^{-k^2 \langle X_m^2 \rangle} \sin(2kG_m) \sum_{n=0}^M \operatorname{Re} (I_{mn,nm}), \quad (42)$$

$$B = 4 \sum_{n=0}^M \operatorname{Re} (I_{mn,nm}) (Q_n^2 - Q_m^2), \quad (43)$$

$$C = -4 \sum_{n=0}^M \operatorname{Re} (I_{mn,nm}) Q_n^2 \sin(2kG_n) e^{-k^2 \langle X_n^2 \rangle}. \quad (44)$$

According to Eq. (39), l.h.s. = A. This means that l.h.s. = r.h.s. if term A dominates in sum (41).

According to Eq. (27), the mean intensity  $\langle |a_m|^2 \rangle$  varies at ranges where  $k^2 \langle X_m^2 \rangle = O(1)$ . It can be shown that at these ranges and at sufficiently large  $k$  the term A dominates in the sum (41). The smallness of term B is caused by the fact that  $Q_m^2$  is a smooth function of the mode number  $m$ . Analysis of Eqs. (33) and (37) shows that the values of  $\Delta_{mn,nm}$  and  $I_{mn,nm}$  decrease with increasing  $|n-m|$  and the main contributions to sums (42) and (43) come from terms with  $n$  belonging to some interval  $|n-m| < \Delta m$ . Consider Brillouin waves with grazing angles close to some fixed value. It is easy to show that the numbers  $m$

of corresponding modes grow with frequency but the values of  $Q_m$  and  $\Delta m$  for these modes will be approximately constant. It means that  $|Q_{m+\Delta m}^2 - Q_m^2|/Q_m^2 = O(1/k)$  and therefore in the high frequency limit the ratio  $B/A$  tends to zero.

The smallness of  $C$  compared to  $A$  is caused by the presence in Eq. (44) a rapidly oscillating factor  $\sin(2kG_n)$ . This can be shown by transforming sum (44) in the same manner as it has been done for sum  $\sum_n \text{Re } I_{mn,nm}$ .

## V Numerical example

In this Section we present results of numerical simulation demonstrating the applicability of Eq. (14) and estimates of statistical moments obtained using this formula. As in Ref. [8] we consider a deep-water waveguide with the canonical sound speed profile and perturbation  $\delta c(r, z)$  induced by random internal waves.

### A Environmental model and numerical simulation

In numerical simulations presented below we use an environmental model with an unperturbed sound speed profile representing the canonical (or Munk) profile [1, 2]

$$\bar{c}(z) = c_r [1 + \varepsilon (e^\eta - \eta - 1)], \quad \eta = 2(z_a - z)/B \quad (45)$$

with parameters  $c_r = 1.5$  km/s,  $\varepsilon = 0.0057$ ,  $B = 1$  km, and  $z_a = 1$  km. This  $\bar{c}(z)$  is shown in the left panel of Fig. 1. The bottom was set at a depth of 5 km.

It is assumed that the weak perturbation  $\delta c(r, z)$  is caused by random internal waves with statistics determined by the empirical Garrett-Munk spectrum [1]. To generate realizations of a random field  $\delta c(r, z)$  we apply a numerical technique developed by J. Colosi and M. Brown [23]. In their model the perturbation has the form

$$\delta c(r, z) = c_r \frac{\mu}{g} N^2 \zeta(r, z), \quad (46)$$

where  $g = 9.8$  m/s<sup>2</sup> is the gravitational acceleration,  $\mu = 24.5$  is a dimensionless constant,  $N(z) = N_0 \exp(z/L)$  is a buoyancy frequency profile,  $N_0 = 2\pi/(12 \text{ min}) = 0.0087$  1/s is a buoyancy frequency near the surface,  $L = 1$  km. The random function  $\zeta(r, z)$  presents internal-wave-induced vertical displacements of a fluid parcel. Its realizations have been computed using Eq. (19) from Ref. [23]. We consider an internal wave field formed by

30 normal modes and assume its horizontal isotropy. Components of wave number vectors in the horizontal plane belong to the interval from  $2\pi/100 \text{ km}^{-1}$  to  $2\pi/2 \text{ km}^{-1}$ . An rms amplitude of the perturbation scales in depth like  $\exp(3z/2L)$  and its surface-extrapolated value in our model is about 0.5 m/s.

All the calculations were carried out at a carrier frequency of 100 Hz. The point source exciting the wave field was set at the sound channel axis  $z = z_a$ . The complex amplitude of the wave field was computed using the method of wide angle parabolic equation for 360 realizations of random perturbation  $\delta c(r, z)$ . Parabolic equation was solved by applying the Crank–Nicolson finite-difference scheme [18]. For each realization of  $\delta c(r, z)$ , the complex amplitude of the sound field was computed up to 500 km. Starting field at  $r = 0$  was generated using the modal starter [18]. Values of  $a_m$  at 501 range points uniformly sampling the interval from 0 to 500 km were found by projecting the computed sound field onto eigenfunctions  $\varphi_m(z)$ . Functions  $a_m(r)$  obtained this way we call the pe-based estimates of mode amplitudes.

Our attention was restricted to amplitudes of the first 66 modes which describe sound waves propagating at grazing angle  $|\chi| < 11.6^\circ$ . Turning points of these modes are located within the water bulk and far enough from the boundaries for the applicability of quantization rule (4). Starting intensities  $|a_m(0)|^2$  of some of these modes are shown by circles in Fig. 2. Numbers of modes whose statistical moments will be shown on the plots presented below, are indicated next to the corresponding circles.

Functions  $X_m^+(r)$  and  $X_m^-(r)$  determined by Eq. (16) were computed for the same 360 realizations of  $\delta c(r, z)$  at the same 501 range points. Then, substituting these functions in Eq. (14) we obtained the ray-based estimates of  $a_m(r)$ .

Thus, in each of 360 realizations of  $\delta c(r, z)$  for each of the first 66 modes we computed a pe-based and ray-based estimate of mode amplitude  $a_m(r)$ . For most modes these two estimates of  $a_m(r)$  are in reasonable agreement. Figure 3 present typical examples of  $|a_m(r)|$  computed these two ways for the same realization of perturbation.

## B Statistical moments of $a_m$

In the remaining part of this paper we will compare the pe-based and ray-based estimates of statistical moments calculated using the Monte Carlo method. In what follows, the angular brackets  $\langle \dots \rangle$  denote the averaging over the 360 realizations of perturbation  $\delta c$ .

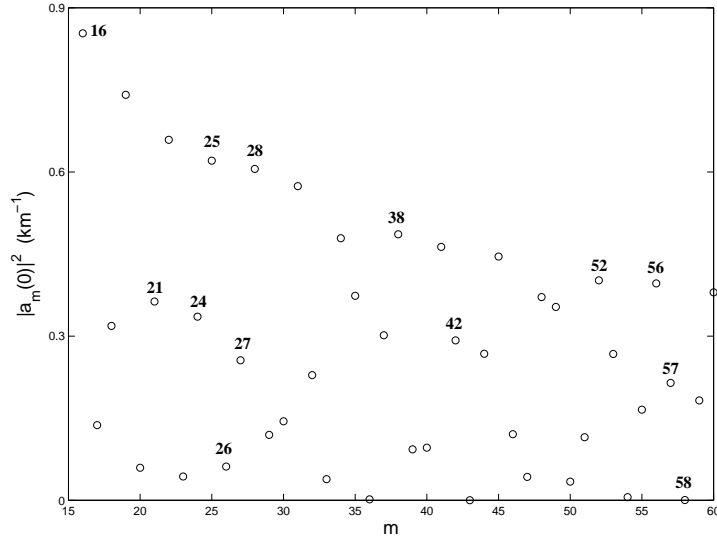


Figure 2: Starting intensities  $\langle |a_m(0)|^2 \rangle$  of normal modes with  $m = 16, \dots, 60$  at a carrier frequency of 100 Hz excited by a point source set at a depth of 1 km.

The ray-based estimates of statistical moments can be obtained in two ways. First, we can substitute functions  $X_m^\pm(r)$  computed for different realizations of  $\delta c$  into formula (14) and average a product of mode amplitudes over all the realizations. Second, we can find the second moments of  $X_m^\pm(r)$  by averaging over the realizations and substitute these moments in Eqs. (17)–(20). Both methods give close results. Therefore below we present only the estimates by the first method.

Figure 4 shows the mean values (coherent components) of complex mode amplitudes  $\langle a_m \rangle$  as functions of range  $r$ . Comparison with similar dependencies for non-averaged mode amplitudes presented in Fig. 3 show that the averaging makes the pe-based and ray-based results more close.

As is seen in Fig. 2, the starting mode intensity  $|a_m(0)|^2$  is a rapidly oscillating function of the mode number  $m$ . For  $m > 3$  the values of  $|a_m(0)|^2$  in our example are well approximated by the WKB relation

$$|a_m(0)|^2 = 2Q_m^2 [1 - \sin(2kG_m)]. \quad (47)$$

According to this formula, the oscillations are caused by term  $\sin(2kG_m)$ . In Eqs. (19) and



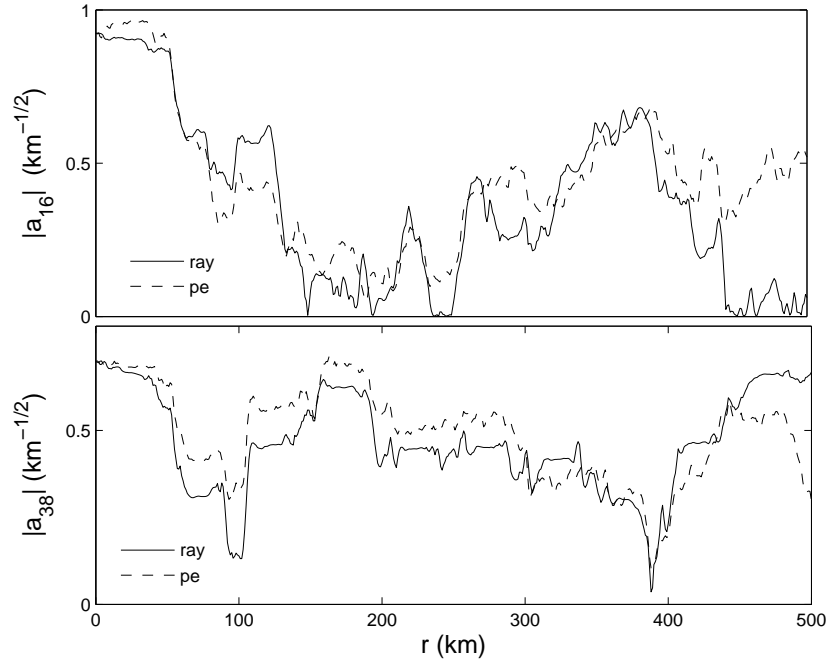


Figure 3: Amplitudes  $|a_m|$  of the 16-th (upper panel) and 38-th (lower panel) modes as functions of range in a single realization of a fluctuating waveguide. The ray-based estimate predicted by Eq. (14) (solid line) is compared to result obtained by modal decomposition of the sound field computed by the method of wide-angle parabolic equation (dashed line).

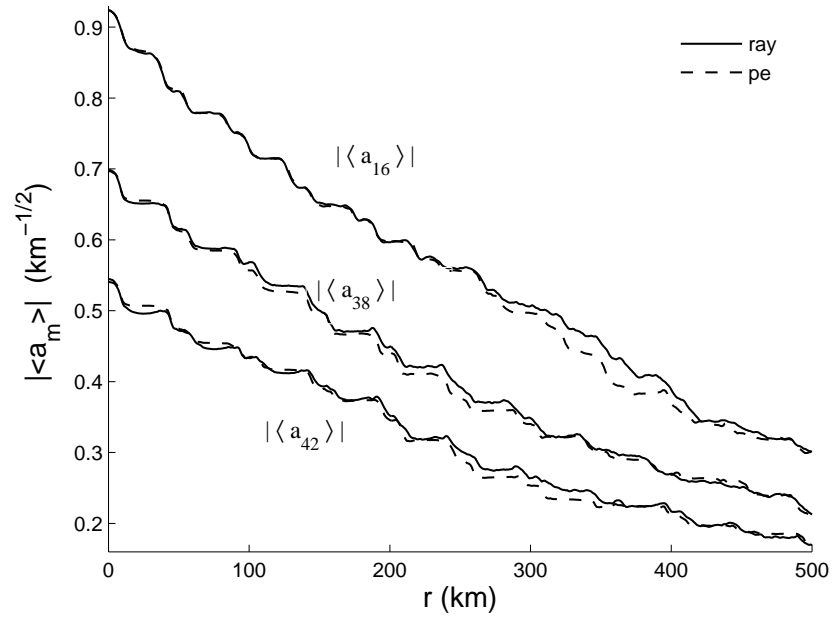


Figure 4: Ray-based (solid lines) and pe-based (dashed lines) estimates of mean mode amplitudes  $|\langle a_m \rangle|$  for  $m = 16$  (upper lines), 38 (middle lines), and 43 (lower lines).

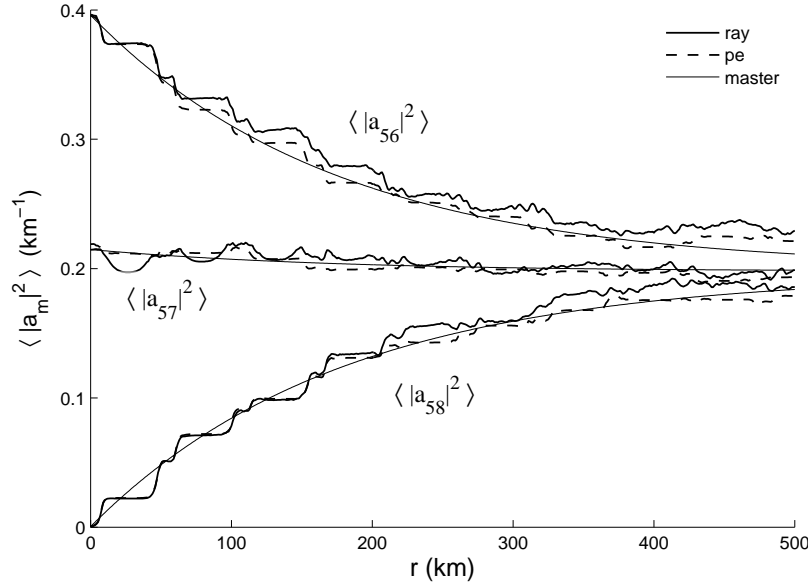


Figure 5: Mean mode intensities  $\langle |a_m|^2 \rangle$  as functions of range for  $m = 56, 57$ , and  $58$ . The ray-based results, pe-based results, and solutions of the master equations are shown by thick solid, thick dashed, and thin solid lines, respectively.

(27) the mode coupling manifests itself in the appearance of a weight factor at  $\sin(2kG_m)$  which monotonically decreases with range. It means that mean intensities of modes with the numbers close to  $m$  monotonically approaches to  $2Q_m^2$ . The equalization of mean mode intensities is clearly seen in Fig. 5 where the range dependencies of mean intensities for modes 56, 57, and 58 are shown. Note that the pe-based (thick solid) and ray-based (thick dash) simulations give results close to each other and to the solution of master equations (32) (thin solid). In accord with results of Ref. [8–10] and our result derived in Sec. IV, the solution of Eqs. (32) gives only a smoothed range dependence of the mean mode intensity  $\langle |a_m|^2 \rangle$  and does not describe its small oscillations.

The presence of these oscillations was predicted in Ref. [12]. From the viewpoint of our ray-based approach they are caused by the fact that the strength of the sound speed fluctuations decreases with depth and therefore the main contributions to integrals (15) come from inhomogeneities located in the vicinities of upper turning points of the mode rays. Near-step-like jumps of  $X_m^\pm(r)$  occur at the mode rays' upper turning points. The

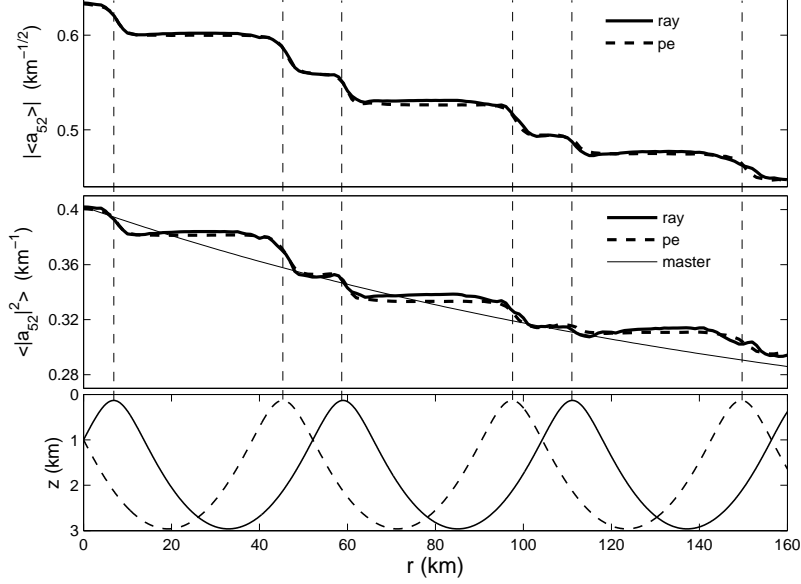


Figure 6: Upper panel: mean amplitude of the 52-nd mode as a function of range. Middle panel: mean intensity of the 52-nd mode as a function of range. Lower panel: mode rays of the 52-nd modes. Thick solid and thick dashed lines in the upper and middle panels show the ray-based and pe-based results. Thin solid line in the middle panel presents the mean intensity  $\langle |a_{52}|^2 \rangle$  found by solving master equations (32).

same is true for the random increment  $X(r)$  of eikonal of any geometrical ray described by Eq. (13). This fact is well known and it underlies the so-called apex approximation [1]. In our example this effect is most pronounced for steep enough rays with grazing angles at the sound channel axis exceeding  $5^\circ$ . These rays form modes with numbers  $m \geq 12$ .

According to Eqs. (17) – (19) the jump-like variations of  $X_m^\pm(r)$  at mode rays' upper turning points cause jump-like variations of statistical moments at the corresponding distances. This phenomenon is illustrated in Fig. 6 where the range dependencies of the mean amplitude (upper panel) and mean intensity (middle panel) of the 52-nd mode are shown. Dashed vertical lines indicate ranges corresponding to upper turning points of mode rays of the 52-nd mode depicted in the lower panel.

Formulas (25)–(28) are derived using the approximation of  $\langle (X_m^\pm(r))^2 \rangle$  by the smooth

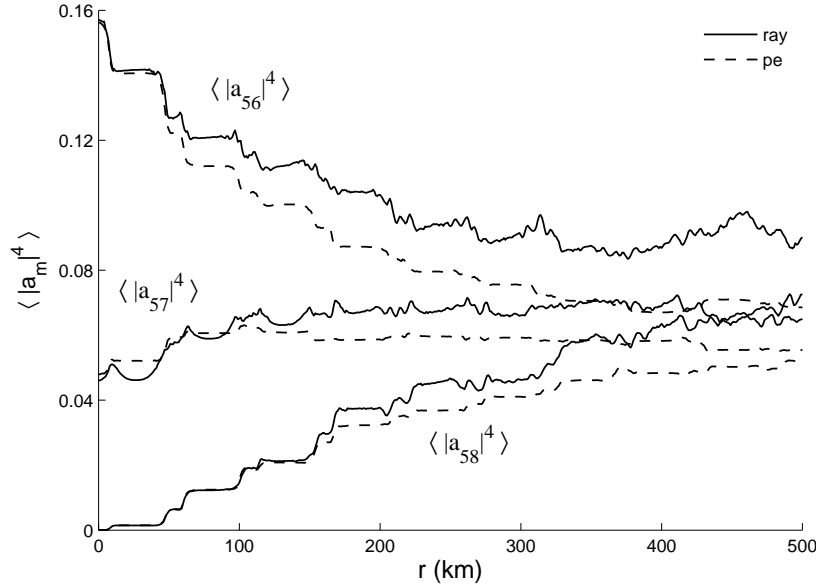


Figure 7: Squared mode intensities for the same normal modes as in Fig. 5. The ray-based and pe-based results are shown by solid and dashed lines, respectively.

function  $\langle X_m^2(r) \rangle$  which has no jumps at the upper turning points of mode rays. This explains why the master equations (32), whose solutions (in the high frequency approximation) are given by Eq. (27), do not predict the small oscillations of mean mode intensities  $\langle |a_m(r)|^2 \rangle$ .

Figure 7 presents the mean squared intensities of the same modes as in Fig. 5. It is seen that the agreement between the ray-based and pe-based estimates for the fourth moments of the mode amplitudes is less good than for the second moments.

## C Cross-correlations of normal modes

According to Eqs. (18), the decorrelation of modes  $m$  and  $n$  is determined by functions

$$Y_{m,n}^{\pm}(r) = \exp \left( -\frac{k^2}{2} \left\langle [X_m^{\pm}(r) - X_n^{\pm}(r)]^2 \right\rangle \right). \quad (48)$$

We will call  $Y_{m,n}^{\pm}$  the correlation functions of mode rays. Figure 8 presents the values of  $Y_{mn}^+$  at 125 (upper panel), 250 (middle panel), and 500 km (lower panel). Functions  $Y_{mn}^-$  have close values (not shown). Let us assume that modes  $m$  and  $n$  are correlated if  $Y_{m,n}^+ > 0.6$ .

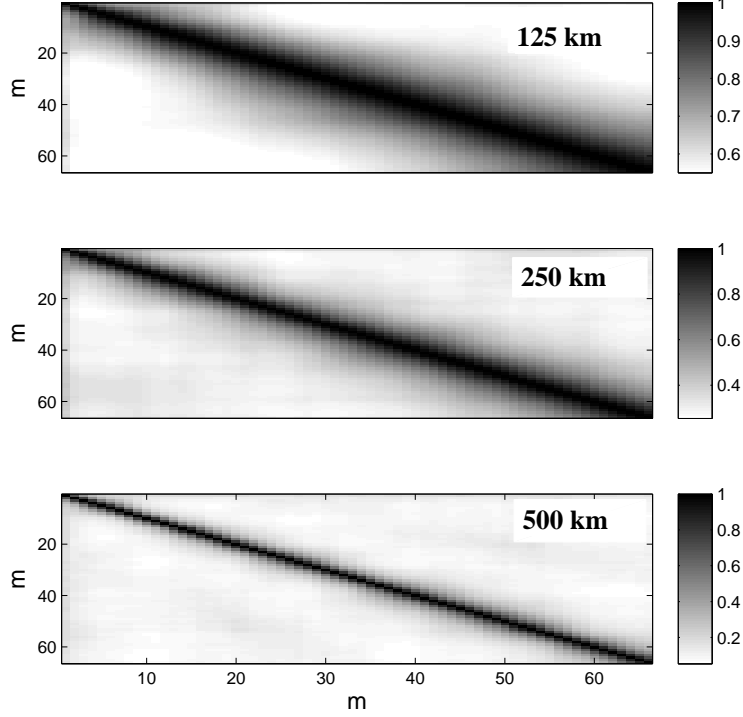


Figure 8: Correlation functions of mode rays  $Y_{mn}^+$  (Eq. (48)) at ranges 125 km (upper panel), 250 km (middle panel), 500 km (lower panel).

Then in Fig. 8, we see that at 125 km a typical mode correlates with 20-40 neighboring modes, at 250 km the number of correlated modes reduces to 10-20, and at 500 km to 3-5.

Correlation functions of mode rays  $Y_{m,n}^\pm(r)$  monotonically decrease with increasing  $r$  and  $|m - n|$ . But, according to Eqs. (18) and (26), the dependencies of joint statistical moments  $\langle a_m a_n^* \rangle$  on  $r$  and  $|m - n|$  can be more complicated. In the analysis of the cross-mode coherence, as in Refs. [8–10], we will consider the normalized joint moments of mode amplitudes  $\langle b_m b_n^* \rangle$ , where

$$b_m(r) = \frac{a_m(r)}{\langle |a_m(r)|^2 \rangle^{1/2}}.$$

In the upper panel of Fig. 9 we present the range dependencies of cross-mode correlations

for modes with very different starting amplitudes at  $r = 0$  (cf. Fig. 2). Joint moments  $|\langle b_m b_n^* \rangle|$  of such modes within some range intervals may grow with range  $r$  and increase with increasing  $|m - n|$ . In our example we see that  $|\langle b_{25} b_{27}^* \rangle|$  grows in the interval from 100 to 400 km, and  $|\langle b_{25} b_{28}^* \rangle|$  exceeds  $|\langle b_{25} b_{26}^* \rangle|$  and  $|\langle b_{25} b_{27}^* \rangle|$ .

Generally, the joint moment  $\langle b_m b_n^* \rangle$  approaches  $Y_{m,n}^\pm(r)$  only at long enough ranges where the factors  $\exp\left(-\frac{k^2}{2} \langle (X_m^\pm)^2 \rangle\right)$  become small. But Eq. (26) suggests that there are modes whose moments  $\langle b_m b_n^* \rangle$  are close to  $Y_{m,n}^\pm(r)$  at any  $r$ . These are the modes with

$$2kG_m \simeq \pi + 2\pi J, \quad (49)$$

where  $J$  is an integer. Indeed, for modes  $m$  and  $n$  satisfying this condition,  $\sin(k(G_m + G_n)) \simeq 0$  and  $\cos(k(G_m - G_n)) \simeq 1$ . Then from Eqs. (27) and (47), it follows that

$$\langle b_m b_n^* \rangle \simeq e^{-\frac{k^2}{2} \langle (X_m - X_n)^2 \rangle} \simeq Y_{m,n}^\pm(r). \quad (50)$$

The lower panel of Fig. 9 present normalized joint moments of such modes. It is seen that these moments  $|\langle b_m b_n^* \rangle|$  are reasonably well approximated by the corresponding correlation functions  $Y_{mn}^\pm(r)$ .

Notice that in the case of adiabatic perturbation, formula (50) is applicable for all the modes. Indeed, the adiabaticity of  $\delta c(r, z)$  requires that  $\Delta_\zeta \gg D_m$ . If this condition is met (in our theory and numeric example we deal with the inverse inequality), then  $X_m^+(r) = X_m^-(r)$  and Eq. (14) translates to

$$a_m(r) = \varphi_m(z_0) e^{ikX_m(r)}. \quad (51)$$

Equation (50) follows immediately from this formula. Thus, it turns out that even though the adiabatic approximation in our example is not applicable, the normalized cross-mode correlations  $\langle b_m b_n^* \rangle$  for modes satisfying condition (49) are properly described using a simple adiabatic formula. It is worthwhile to note, that the starting intensities of modes satisfying condition (49) are  $|a_m(0)|^2 \simeq 2Q_m^2$  and their mean intensities weakly vary with range (see the preceding subsection), that is, they behave like the intensities of adiabatic modes.

## VI Conclusion

In this paper the predictions of our ray-based analytic approach are compared with results of full wave numerical simulation. Figures 3–7 and 9 present results of this comparison

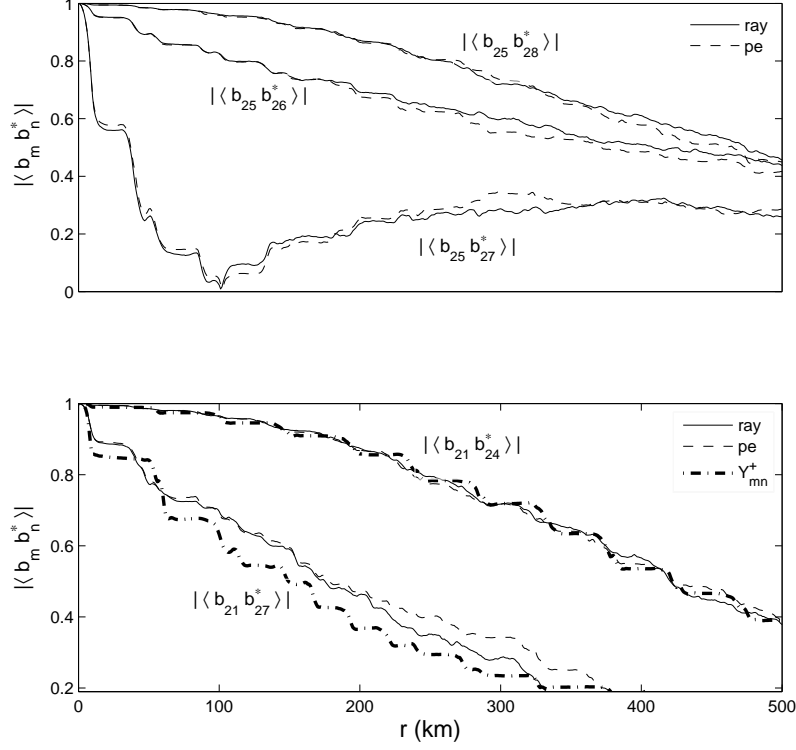


Figure 9: Cross-mode coherences  $|\langle b_m b_n^* \rangle|$  as functions of range. Coherences for mode pairs (25,26), (25,27), and (25,28) are shown in the upper panel; for mode pairs (21,24) and (21,27) are shown in the lower panel. In both panels, the ray-based and pe-based results are shown by thin solid and thin dash lines, respectively. In the lower panel, the correlation functions of mode rays  $Y_{mn}^+$  (Eq. (48)) are shown by thick dot-dashed lines.



which are typical for most modes with numbers  $m \leq 66$ . The comparison has confirmed the applicability of our approach for the analysis of mode coupling in a deep water waveguide with sound speed fluctuations induced by random internal waves. At a frequency of 100 Hz it can be used at ranges of a few hundred kilometers. However, for some modes, especially for those which are weakly excited by the source and have small initial amplitudes, the coincidence between the ray-based and pe-based estimates may be much worse (not shown).

Since our approach is based on the WKB approximation, even at high frequencies it cannot be used for those modes whose turning points are located in the vicinity of the source depth or in the water bulk near the surface or bottom. We have avoided these problems by setting the source at the sound channel axis and restricting our attention to modes with turning points located well below the surface and above the bottom. The WKB approximation and, hence, our approach can be applied for modes with turning points on the waveguide boundaries. But in the present paper such modes were not considered.

Numerical simulation has confirmed the prediction of Ref. [12] that the range-dependencies of mode intensities and other statistical moments are not smooth. They manifest jump-like changes at ranges corresponding to upper turning points of the mode rays.

Important advantage of our approach is its applicability for evaluating the cross-correlations of mode amplitudes at different frequencies needed for treating pulse propagation. It is clear that analytical estimates for mode amplitudes at different frequencies are readily derived along the same lines as estimates for statistical moments given by Eqs. (17)–(20). But this issue goes beyond the scope of the present work and it is not broached here.

It should be emphasized that formula (14) is derived under assumption that in the presence of perturbation the ray paths do not deviate from their unperturbed positions. This assumption is valid only at short enough ranges. In subsection V.B it is shown that the mode coupling causes the equalization of mean mode intensities. According to Eqs. (19) and (27) mean intensities  $\langle |a_m(r)|^2 \rangle$  of modes with numbers close to  $m$  approach  $2Q_m^2$ . Numerical simulation confirms this prediction (see Fig. 5). However, our approach cannot describe subsequent changes of mode intensities with distance. In particular, it cannot be used to study establishing the equipartition of energy among the modes in the limit  $r \rightarrow \infty$  predicted in Ref. [4].

In Sec. IV, a numerical result of Refs. [8–10] that the master equations properly describe smoothed range-dependencies of mean mode intensities is explained from the view point of our ray-based approach. It is shown that formula (27) for the mean mode intensity obtained

by smoothing the range-dependent parameters of Eq. (19) over the cycle of the mode ray gives an approximate solution of the master equations valid in the high frequency limit.

We assume that the expressions for  $\langle a_m a_n^* \rangle$  given by Eq. (18) represent an approximate solution of the complete system of  $M^2$  equations for these joint moments derived in the Markov approximation in Refs. [6, 8]. However, for now, this assumption has not been verified by direct substitution of Eqs. (18) in this system.

In Refs. [9, 10], it is shown for a shallow water waveguide, that the analytic expression for the joint moment  $\langle b_m b_n^* \rangle$  with  $m \neq n$  derived in the adiabatic approximation may be valid if the sound speed fluctuations are non-adiabatic. In the present paper, this issue has not been studied in detail. However, we hope that our comment on applicability of the adiabatic results in a non-adiabatic environment made at the end of subsection V.C may contribute to understanding this result of Refs. [9, 10].

Finally, note that Eq. (14) for the mode amplitude and the expressions for statistical moments following from this formula can be easily generalized to the case of a range-dependent unperturbed waveguide. This can be done using analytical relations expressing mode amplitudes in a range-dependent waveguide through parameters of ray paths [20–22].

## Acknowledgment

The work was partially supported by the Program “Fundamentals of acoustic diagnostics of artificial and natural media” of Physical Sciences Division of Russian Academy of Sciences, Grants No. 13-02-00932 and 13-02-97082 from the Russian Foundation for Basic Research, and Leading Scientific Schools grant N 339.2014.2.

## References

- [1] S.M. Flatte, R. Dashen, W.M. Munk, K.M. Watson, and F. Zakhariassen, *Sound transmission through a fluctuating ocean* (Cambridge U.P., London, 1979), Chaps. 7, 8, 11.
- [2] L.M. Brekhovskikh and Yu.P. Lysanov, *Fundamentals of Ocean Acoustics* (Springer-Verlag, New York, 2003), Chaps. 6, 10.

- [3] W. Kohler and G.C. Papanicolaou, “Sound propagation in a randomly inhomogeneous ocean,” in *Lecture Notes in Physics. V. 80. Wave propagation and underwater acoustics*, edited by J.B.Keller and J.S.Papadakis (Springer-Verlag, Berlin, 1977), pp. 153-223.
- [4] L.B. Dozier and F.D. Tappert, “Statistics of normal mode amplitudes in a random ocean. I. Theory ”, J. Acoust. Soc. Am., **63**, 353–365 (1978).
- [5] L.B. Dozier and F.D. Tappert, “Statistics of normal mode amplitudes in a random ocean. II. Computations”, J. Acoust. Soc. Am., **64**, 533–547 (1978).
- [6] D.B. Creamer, “Scintillating shallow-water waveguides,” J. Acoust. Soc. Am., **99**, 2825–2838 (1996).
- [7] A.G. Sazontov, A.L. Matveyev, and N.K. Vdovicheva, “Acoustic coherence in shallow water: Theory and observation,” IEEE J. Ocean. Eng., **27**, 653–663 (2002).
- [8] J.A. Colosi and A.K. Morozov, “Statistics of normal mode amplitudes in an ocean with random sound-speed perturbations: Cross-mode coherence and mean intensity,” J. Acoust. Soc. Am., **126**, 1026–1035 (2009).
- [9] J.A. Colosi, T.F. Duda, and A.K. Morozov, “Statistics of low-frequency normal-mode amplitudes in an ocean with random sound-speed perturbations: Shallow-water environments,” J. Acoust. Soc. Am., **131**, Pt. 2, 1026–1035 (2012).
- [10] K. Raghukumara and J.A. Colosi, “High frequency normal mode statistics in a shallow water waveguide: The effect of random linear internal waves,” J. Acoust. Soc. Am., **136**, 66-79 (2014).
- [11] A.L. Virovlyanskii and A.G. Kosterin, “Method of smooth perturbation for the description of the fields in multimode waveguides” (in Russian), Akust. Zh. **33**, 599-605 (1987); English transl.: Sov. Phys. Acoust., **33**, 351–354 (1987).
- [12] A.L. Virovlyanskii, A.G. Kosterin, and A.N. Malakhov, “Mode fluctuations in a canonical underwater sound channel” (in Russian), Akust. Zh. **35**, 229-235 (1989); English transl.: Sov. Phys. Acoust., **35**, 138–142 (1989).

- [13] A.L. Virovlyanskii, “Correlations of modes in a waveguide with large-scale random inhomogeneities” (in Russian), *Izv. Vuzov Radiofizika* **32**, 832-838 (1989); English. transl.: *Radiophysics and Quantum electronics*, **32**, 619–624 (1989).
- [14] A.L. Virovlyansky, A.G. Kosterin, and A.N. Malakhov, “Fresnel zones for modes and analysis of field fluctuations in random multimode waveguides,” *Waves in Random Media*, **1**, 409–481 (1991).
- [15] A.L. Virovlyansky, V.V. Kurin, N.V. Pronchatov-Rubtsov, and S.I. Simdyankin, “Fresnel zones for modes,” *J. Acoust. Soc. Am.*, **101**, 163–173 (1997).
- [16] A.G. Voronovich and V.E. Ostashev, “Low-frequency sound scattering by internal waves in the ocean,” *J. Acoust. Soc. Am.*, **119**, 1406–1419 (2006).
- [17] A.G. Voronovich and V.E. Ostashev, “Coherence function of a sound field in an oceanic waveguide with horizontally isotropic statistics,” *J. Acoust. Soc. Am.*, textbf125, 99–110, (2009).
- [18] F.B. Jensen, W.A. Kuperman, M.B. Porter, and H. Schmidt, *Computational Ocean Acoustics* (Springer, New York, 2011), Chaps. 5,6.
- [19] W. Munk and C. Wunsch, “Ocean acoustic tomography: A scheme for large scale monitoring”, *Deep-Sea Res.*, **26**, 123–161 (1979).
- [20] A.L. Virovlyansky, and G.M. Zaslavsky, “Wave chaos in terms of normal modes,” *Phys. Rev. E*, **59**, 1656-1668 (1999).
- [21] A.L. Virovlyansky, A.Yu. Kazarova, and L.Ya. Lyubavin, ”Ray-based description of normal mode amplitudes in a range-dependent waveguide,” *Wave motion*, **42**, 317–334 (2005).
- [22] D. Makarov, S. Prants, A. Virovlyansky, and G. Zaslavsky. *Ray and wave chaos in ocean acoustics* (Word Scientific, New Jersey, 2010), Chap.3, pp. 150-168.
- [23] J.A. Colosi and M.G. Brown, “Efficient numerical simulation of stochastic internal-wave-induced sound-speed perturbation field,” *J. Acoust. Soc. Am.*, **103**, 2232–2235 (1998).